Section – Geotechnical Engineering and Construction

Geophysical Monitoring of Underground Constructions and its Theoretical Basis

Michael Ezersky[1,*], Lev Eppelbaum[2]

[1] Geotec Engineering and Environmental Geophysics Ltd, P.O.B. 25031, Rishon Lezion 7502501, Israel

[2] School of Geosciences, Raimond and Beverly Sackler Faculty of Exact Sciences, Tel Aviv University, Ramat Aviv, 6997801, Tel Aviv, Israel

Abstract: To avoid damage of rock mass, their collapse into underground space, danger for equipment and risks for human life, during construction and exploitation of large engineering projects (e.g. underground spaces, tunnels, machine halls, etc.) in-situ geotechnical and geophysical monitoring is carried out. Geophysical monitoring is based on observations of the elastic shear- and longitudinal wave velocities (Vs and Vp, respectively) and Acoustic Emission (AE). The behaviors of the elastic velocities and parameters of AE during rock deformation depend on the types of the future failure that, in turn, are defined by the structure and properties of the medium and characteristics of stress state σ_3/σ_1 and hydrostatic pressure. These velocity variations are defined by difference in effective parameters of forming microfractures, whose geometry is distinguished at different modes of stress state. At that character of interaction between microfractures determines the types of the macrofailure. In this study, we discuss the behaviors of longitudinal wave velocities and acoustic emission during loading of large rock blocks and underground opening orienting measurements along maximum (σ_1) and minimum (σ_3) stresses. It is shown that velocity variations along the maximum stress is more informative at elastic phase of rock deformations (velocity increases), whereas velocity variations along axis of the minimum stress is more informative at the stage of nonlinear rock deformation (velocity begins to decrease during microfractures occurrence). These regularities are well observed at unloading rock mass in the Zhinvali tailrace tunnel where geophysical monitoring assisted in the construction. This knowledge could be used in planning and monitoring the stability of underground structures.

Keywords: monitoring, P- and S-wave velocity, stress state, tunnels, underground halls

1 Introduction

Construction and exploitation of large underground complexes at seismic tectonically active regions resulted in intensive deformation processes at the shallow subsurface, which could be reason of the serious accidents (Drescher and Handley 2003, Da Gama 2004, Jaeger et al 2007, Maghsoudi and Kalantari 2014, Roberts et al 2015). Apart from this, creation of underground opening within stressed rock mass modifies their stress state (Zienkiewicz 1968, Rock Engineering Book 1997, Zienkiewicz et al 2014). Therefore, the construction of underground complexes with extended tunnels of tens kilometer long and more than 10 m in diameter, machine halls of 50–60 m high and some hundreds meters long, and concrete dams of some hundreds meters high require to monitor their stability during construction works (Savich and Kujundjich 1990). Such monitoring based on geophysical parameters using seismic geotomography, ultrasonic and acoustic emission methods have been carried out during the constructions of the high concrete dam Ingury Hydro Power Station (HPS) (Savich et al 1983), large underground openings (Acrimony et al 1987, Ezersky et al 1991a, 1992, 1993b, Yamamoto and Ito 1993, Yu et al 2005,

Philips et al 2015), repositories (Barta et al 2014, 2016) and tunnels (Ezersky et al 1993a, Luth et al 2014, Maghsoudi and Kalantari 2014). This monitoring is based on exact knowledge of the regularity of geophysical parameters at all stages of rock deformation process from elastic deforming to failure (Pacher 1970). The scale effects on acoustic parameters in rocks also have been studied (Savich and Kujundjich 1990, Ezersky and Goretsky 2015).

The present work is a continuation of Ezersky (2017). It is aimed to study in details the behaviors of the longitudinal wave velocities (V_P) and acoustic emission (AE) inside the zones of the forming of both shear and tensile macro fractures during loading to failure of large rock blocks. Behaviors of acoustic parameters in the rock samples during their deforming from zero to failure have been described in Ezersky (1985). The results have been used in design, construction and monitoring large underground structures such as Inguri Hydro Power Station (HPS) in Georgia (Savich et al 1983), Rogun Underground Machine Hall (MH) in Tajikistan (Ezersky et al 1991a), and Hoabinh Underground MH in Vietnam (Ezersky et al 1993b, Ezersky 2017). In this paper, we present results of monitoring carried out in the tailrace tunnel of the Zhinvali Project in Georgia.

---

* Corresponding Author: Michael Ezersky, email: mikhail@geotec.co.il, Tel: +972-3-6227-334

2 Major Regularities of Rock Failure based on Large Scale Investigations

Numerous studies on rock samples have shown that failure of the polycrystalline medium such as rocks is not an instant process. It develops in some time sequence and accumulation and interaction of the microfractures result in formation of macrofracture (Brace et al 1966). The variations of the physics-mechanics rock properties preceding the failure allow us to use different geophysical methods sensitive to such variations to predict the failure. Among the geophysical methods, seismic-acoustic methods are to monitor different waves spreading in the deformed medium, measure their velocity and attenuation (closely connected with microfractures parameters) (Kuster and Toksöz 1974, Salganik 1979) and record acoustic emission (Scholz 1968, Spies et al 2005, Philipps et al 2015). Our model of rock failure (Ezersky 1985, 2017) is based on the three known models including: (1) Model of Hoek's (1968) failure by macrofracture, (2) statistical model of macrofracture by Stavrogin and Protosenya (1979, 1983), and (3) dependence

of elastic wave velocities on parameters of microfractures (Salganik 1979). Let us consider each one of the models:

(1) Failure, in a strict sense, is failure surfaces forming (Muller 1963). Muller has defined three main rupture modes: rupture by separation, rupture by sliding and rupture by shearing. Hoek (1968) names the first rupture mode as shear failure (Fig. 1a) and the second as tensile failure (Fig. 1b). Stable crack configuration is shown in Fig. 1c. At that the tensile fracture is oriented perpendicularly to the minimum normal stress axis σ_3 ($a_s = 0°$) and shear rupture is oriented by angles between 0 to 45° to σ_1 (the compression is regarded as positive and $\sigma_1 > \sigma_2 > \sigma_3$). We name the rupture surfaces formed after failure as *macrofracture*. The *microfractures* are discontinuities formed from initial defects as a result of a stress acting. It is experimentally proved that at the elastic-plastic and plastic rock behavior its failure takes place as a result of microfractures accumulation, grouping and their interaction at the stresses close to the strength limit.

The avalanche-like failure stage takes place at the critical microfractures density followed by the macrofracture forming (Scholz 1968, Brady 1974).
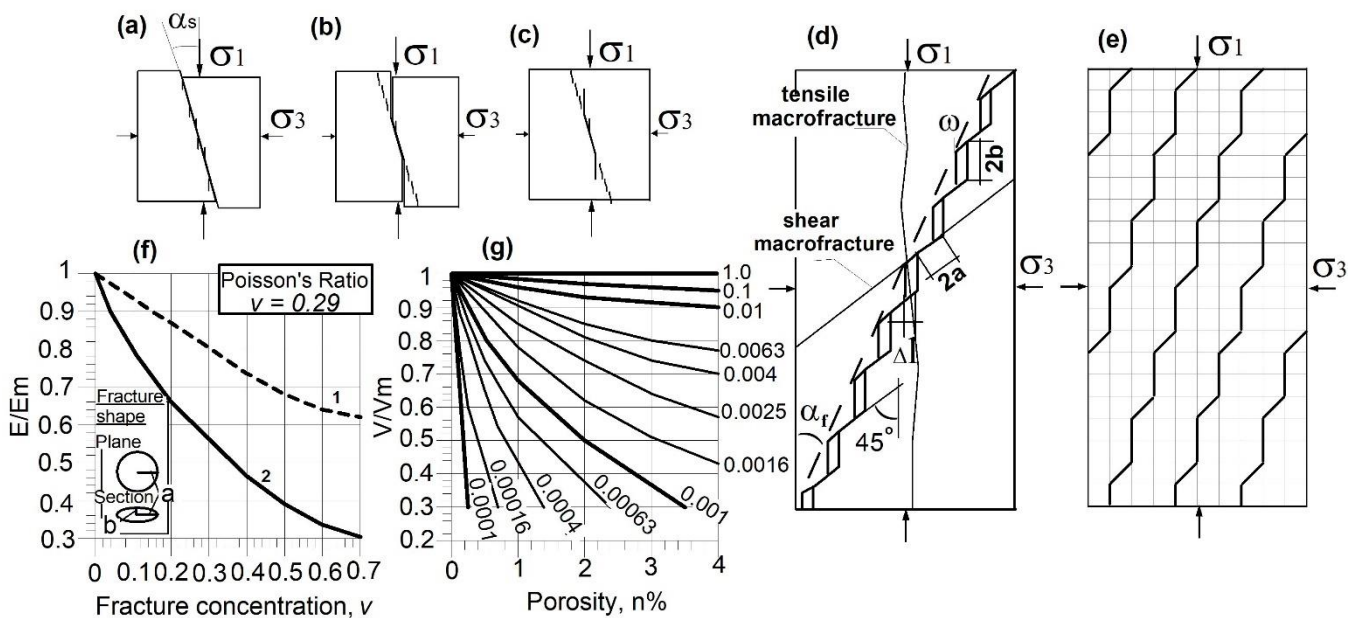
Fig. 1. Suggested rupture modes under compressive stress conditions. (a) Shear failure; (b) Tensile failure; and (c) Stable crack configuration (by Hoek 1968); Model of the shear failure by Stavrogin and Protosenya (1983); (d) shear macrofracture and (e) failure microelements; Model of the solid with numerous fractures. (f) Inter-relations between fractures concentration (υ) and relative velocity (V/V_m) for isotropic (1) and transversally isotropic (2) media; (g) Inter-relations between fractures summary volume (n %) and relative velocity (V/V_m). Curves parameter is the aspect ratio $\alpha = b/a$.

(2) Stavrogin and Protosenya (1979, 1983) have explained the plasticity of rocks under three-axial loads by forming of microfractures manifested in the dilatancy (or inelastic volume increase). They have proposed an universal model of the heterogeneous media shear failure based on numerous experimental data acquired from a wide range of stress state modes. The model explains the dilatancy phenomenon characteristic for all rocks. By analyzing the experimental data, the authors have drawn a conclusion that

it is not possible to explain residual deformations of rock using only shear deforming mechanism. Hypothetic model of macrofracture forming in isotropic heterogeneous material is presented in Fig. 1d. At the failure of the rock sample deformed by the major normal stress σ_1 and $\sigma_2 = \sigma_3$ macroscopic shear plane is formed inclined to the rock axis by angle of a_s (named "failure angle"). It shows from experimental data that the failure angle increases and approaches to 40–45° as stress state mode C = σ_3/σ_1 ratio

increases. The shear macrofracture is represented as combination of the shear and tensile failure micro-planes (elements). The shear microplanes are inclined by an angle of 45° to compression axis (they are inter-grained defects, in first approaching). The tensile microelements are oriented along the compression axis and they can be considered as a microfractures growing from shear element tips like mechanism described by Hoek (1968) (Fig. 1a, b & c). The external stresses cause shear along 2a element and tensile on 2b (Fig. 1d). Then failure angles are depending on the ratio of a and b. At the case $a = b$, failure angle $\alpha_s = 22.5°$, the parameter $x = b/a$ is introduced:

$$x = 0.707 \times (\text{Ctg } a_s - 1) \qquad (1)$$

Parameter x determines the inclination angle of the failure macro plane to main compression axis and, in its turn, it is determined by the stress state mode $C = \sigma_3/\sigma_1$.

From expression (1), at the $\alpha_s = 45°$ parameter x and material is deformed along shear planes coinciding with a plane of maximum shear stress (sliding). At the failure angle $a_s = 0°$ parameter $x = \infty$ and macrofracture is pure tensile crack oriented along compression axis. At the intermediate case (a_s is between 0 and 45°) the macrofracture is combined from shear and tensile elements. Then, shear failure takes place (Fig. 1e). In reality, to get the failure angle of 45° in rocks is practically impossible because of rock heterogeneity (it is very difficult even in soils, especially those coarse and medium grained). The above described model shows the same failure origin and any failure could be considered on this basis.

(3) For description of the dilatancy and failure stages the models of the solid with numerous fractures are used (O'Connel and Budiansky 1974, Salganik 1979). The loaded rock is represented as a homogeneous isotropic or transversal-isotropic solid (or matrix) with elastic modulus E_m (or velocity V_m) including the numerous statistically distributed isolated fractures. Concentration of these fractures uniquely defines the effective elastic characters of the medium E or V. The fracture filling has effective elastic parameters E_f or V_f. It is supposed the fractures are circle in plane and they have a radius a. The fractures have cross-section of the elliptical shape with the half axes of b and a size, as shown in Fig. 1f. The $\alpha = b/a$ ratio is named as the aspect ratio (or shape coefficient). The fracture concentration parameter is defined as $\upsilon = N \times a^3$, where N is the fracture number within single volume (fracture density). The relative effective elastic modulus E/E_m versus fracture concentration υ for isotropic and transversal-isotropic medium (Salganik 1979) are demonstrated in Fig. 1f.

One of the important consequences of this model is that E/E_m parameter (which slightly depends on Poisson's ratio) is a measure of the fracture concentration. The other important consequence is obtained if to connect the velocity variation with a fracture volume. The relative velocity V/V_m versus fractures volume n% is presented in Fig. 1g.

One can see that velocity is dependent on both fracture volume and fracture shape. At the same fracture volume, the long narrow fractures (the aspect ratio is low: for instance, α = 0.001) shows the more considerable velocity decrease than

short or sphere similar fractures (pores) with a high aspect ratio of 0.1–1.0. At the same aspect ratio, the velocity decrease is a measure of the fractures volume. The loading of the rock volume results in an inelastic volumetric deformation (dilatancy), which is the fracture volume variation (Ezersky 1985). So, measuring velocity variations versus inelastic volumetric deformation $\mathcal{E}_v$ (or $\mathcal{E}_3$ axial inelastic deformation) somewhat information about the modal fractures aspect ratio values could be obtained.

Thus, variations of elastic velocities (both Vp and Vs) are determined by variation of parameters of microfractures – volume, geometry (expressed by shape coefficient), etc. During loading rock mass, parameters of microfractures are changed, causing variation of velocities: at compression, they increase and at tensile or tensile with compression, decrease. In its turn, parameters of microfractures define the types of macrofracture.

3   Stress State Around Underground Structures

3.1 In situ stresses

Rocks at depth are subjected to stresses resulting from the mass of the overlying strata, and from stresses of tectonic origin. When an opening is excavated, the stress field is locally disrupted and a new set of stresses are induced in the rock surrounding the opening (Fig. 2). Knowledge of the magnitudes and directions of these stresses is an essential component of the underground excavation design since, in many cases, the strength of the rock is exceeded and the resulting instability can have serious consequences on the behavior of the excavations.

An element of rock at a depth of 1,000 m below the surface is loaded by the weight of the vertical column of rock above this element. It is therefore the product of the depth and the unit weight of the overlying rock mass (typically about 2.7 tons/m^3). Hence the vertical stress on the element is 2,700 tons/m^2 or 27 MPa. This stress is estimated from the simple relationship (Jaeger et al 2007):

$$\sigma_v = \gamma \times z \qquad (2)$$

where σ_v is the vertical stress, γ is the unit mass of the overlying rock, and z is the depth below surface.

The horizontal stresses acting on an element of rock at a depth z below the surface are much more difficult to estimate than the vertical stresses. Normally, the ratio of the average horizontal stress to the vertical stress is denoted by the letter λ such that:

$$\sigma_h = \lambda \sigma_v = \lambda \gamma z \qquad (3)$$

Terzaghi and Richart (1952) suggested that, for a gravitationally loaded rock mass in which no lateral strain is permitted during formation of the overlying strata, the value of λ is independent of depth and is given by $\lambda = \nu (1 - \nu)$, where ν is the Poisson's ratio of the rock mass. This relationship was widely used in the early days of rock mechanics but, as discussed below, it has been proved inaccurate and is barely used today.

3.2 Induced stresses

When an underground opening is excavated into a stressed rock mass, the stresses in the vicinity of the new opening are re-distributed. Consider the example of the stresses induced in the rock surrounding a horizontal circular tunnel (as illustrated in Fig. 2a), showing a vertical slice normal to the tunnel axis. Before the tunnel is excavated, the in-situ stresses σ_v, σ_{h1} and σ_{h2} are uniformly distributed in the slice of rock under consideration. After removal of the rock within the tunnel, the stresses in the immediate vicinity of the tunnel are changed and new stresses are induced. Three principal stresses σ_1, σ_2 and σ_3 acting on a typical element of rock are shown in Fig. 2a.

The convention used in rock engineering is that *compressive* stresses are always *positive* and the three principal stresses are numbered such that σ_1 is the largest compressive stress and σ_3 is the smallest compressive stress or the largest tensile stress of the three abovementioned. According to common consideration, the Strength Factor $F = \sigma_{cr} / \sigma_{ind}$, is used defined by the ratio of rock mass strength (σ_{cr}) to the induced stress (σ_{ind}) at each point (Rock Engineering Book 1997).

New distribution of stresses is shown in Fig. 2b. This distribution depends on the stress level, stress ratio and properties of rocks (Bulychev 1982). Elastic distribution of induced stresses in cylindrical coordinates around the circular tunnel is shown in Fig. 2b (cylindrical coordinates are more conventional presentation of stress state near the tunnels).
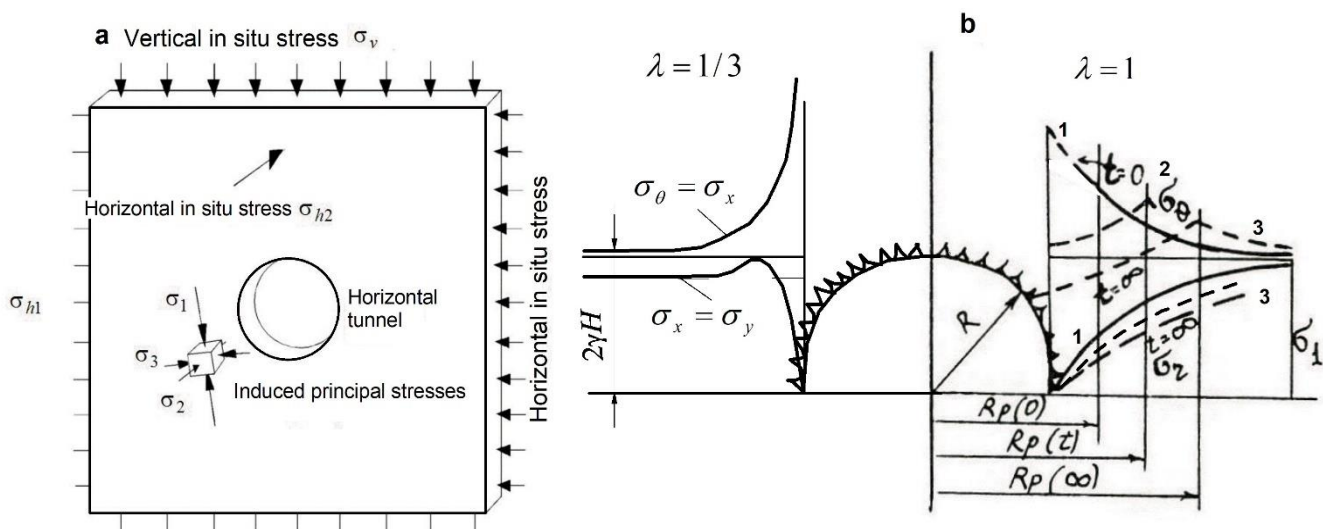
Fig. 2. (a) Illustration of principal stresses induced in an element of rock close to a horizontal tunnel subjected to a vertical in situ stress σ_v, a horizontal in situ stress, σ_{h1} in a plane normal to the tunnel axis and a horizontal in situ stress σ_{h2} parallel to the tunnel axis; (b) Elastic distribution of induced stresses around the circular tunnel in cylindrical coordinates; (c) Temporal variations of distribution of induced stresses in cylindrical coordinates around the circular tunnel: σ_θ – normal tangential stresses; σ_r – normal radial stresses; $Rp(0)$ – unloading radius at the zero time after tunnel excavation; $Rp(t)$ – radius of the unloading zone at the time t; $Rp(\infty)$ – unloading radius at $t = \infty$. (1) elastic stress distribution; (2) plastic-elastic distribution; and (3) viscous–plastic distribution.

Tangential stress σ_θ reaches high values near the tunnel contour and decreases to $\sigma_\theta = \gamma H$ at the distance in several times exceeding the tunnel radius (R). Radial stress which is zero at the tunnel contour, increases with increasing distance from the tunnel and reaches value of $\sigma_r = \lambda\gamma H$. Creating support around the tunnel results in interaction between support and rock that changes the secondary stresses in the rock mass around the tunnel (Bulychev 1982).

Three cases are considered in Fig. 2c: graph 1 presents elastic stress distribution corresponding to high strength factor (low stresses level with respect to strength of rock). If stress concentration σ_θ on tunnel contour has higher values than strength of rock ($F < 1$), zone of plastic deformations is formed close to tunnel. With distance from the tunnel σ_θ decreases and at certain distance $F = 1$ and further elastic stress distribution is remained (curve 2 in Fig. 2c). It is plastic-elastic distribution that corresponds to low stress factor ($F = 0.5$–0.8); 3 – finally, viscous–plastic distribution corresponds to very low strength factor ($F < 0.5$). Radial stress σ_r increases from zero at tunnel contour to stress determined by (2) at the distance in several times exceeding the tunnel radius (R). In rocks characterized by creep, strength decreases with time and maximum σ_θ is removed from the tunnel contour into deep rock mass (curve 3 in Fig. 2c). Radial stress σ_r also decreases comparing with the previous time. Example of stress factor distribution around two types of underground structures (taken from the Rock Engineering Book 1997) is shown in Fig. 3.

Low stress factor ($F < 1$) corresponds to rock plastic deformations, which physically are zones of fractured rocks occurring at failure under the induced stresses. These zones can be identified by geophysical methods based on examination of elastic wave velocities and *acoustic emission* (AE), also named as *microseismic activity* (MSA).
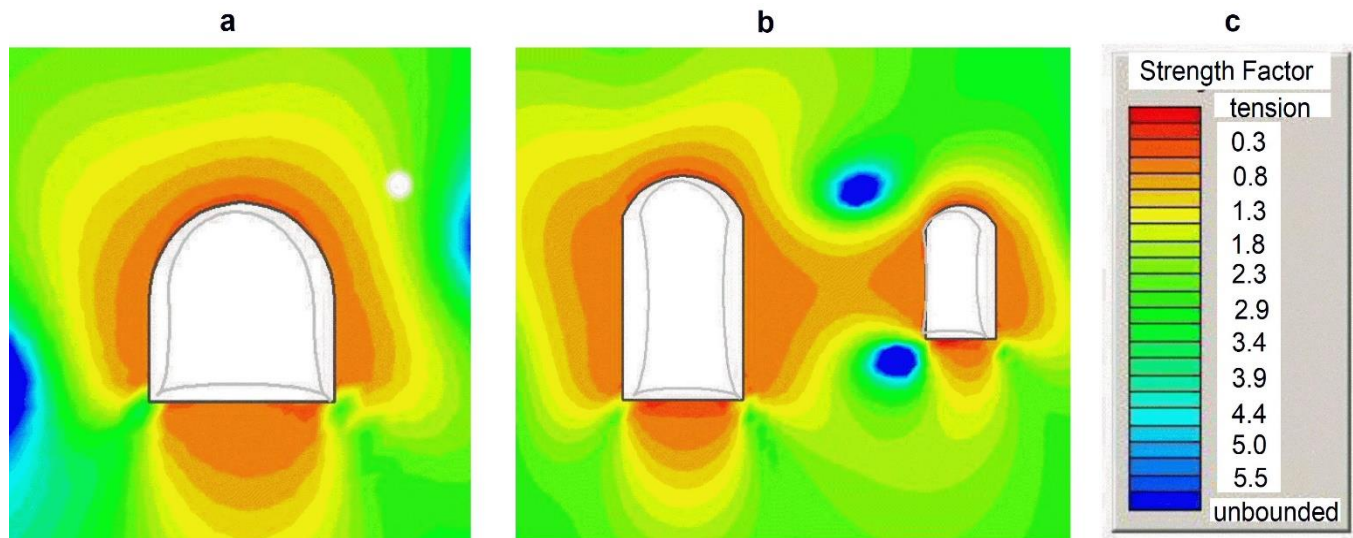
Fig. 3. Comparison of two underground structures: (a) horseshoe tunnel, and (b) powerhouse and transformer gallery layouts, using EXAMINE2D (example is taken from the Rock Engineering Book 1997). The contours are for the Strength Factor defined by the ratio of rock mass strength to the induced stress at each point (c) color scale. The deformed boundary profile (exaggerated) is shown inside the excavation. *In situ stresses*: Major principal stress $\sigma_1 = 10$ MPa; Minor principal stress $\sigma_3 = 7$ MPa; Intermediate stress $\sigma_2 = 9$ MPa; Inclination of major principal stress to the horizontal axis = 15º; *Rock mass properties*: Friction angle $\varphi = 35$º; Cohesion $c = 1$ MPa; Tensile strength = zero; Deformation modulus $E = 4600$ MPa.

4 Geophysical Study of Macrofracture Forming based on Large-scale Tests

In spite of the high level of the modern loading machines and laboratory test equipment for sample testing, it is necessary to study the large volume rocks in situ. It permits to avoid influence of the sample boundaries and loading machines stiffness as well as to study differentially the failure development in the space. Such study enables us to understand regularities of velocities and acoustic emission behaviors in different macrofracture locations of rock mass and in macrofractures of different origin.

4.1 Methods

4.1.1 Shear test of the concrete stamp on rock foundation

Loading scheme

The study was carried out in situ under underground cameras within a 3×3 m² section. The rock mass is composed of effusive rocks which are represented by the clastolavas of basalt porphyrites and their lava breccias. The rocks are discontinued by the joints system which form the blocks of different orders starting from 0.15– 0.20 m. No anisotropy of the elastic properties was found.

The concrete stamp (1) mounted on rock foundation was loaded by the shear load T applied to the frontal plane (1a) and normal load N applied to stamp top. Dividing T and N by square of contact area between the stamp and rock mass we obtain average shear (τ) and normal (σ) stresses at contact zone. The normal load was increased from zero up to N value which was kept constant during the loading test. The shear load was increase by steps ΔT from zero up to ultimate value $T_s(\tau_s)$. The Ratio $T/T_s = \tau/\tau_s$ determines the load level.

Diagrams of displacements of stamp and its frontal and back stamp plains are shown in Fig. 4b.

Total stamp deformations (curve 13 in Fig. 4b from left) demonstrate typical deformation stages (Pacher 1970, Jaeger et al 2007). They are: stage of inelastic deformation connected with a fracture closing (I), quasi elastic linear behavior (II), inelastic deformation (dilatancy stage III) connected with a microfractures opening and development and, at last, failure stage (IV) which includes the microfractures interaction and macrofracture forming which destroys the deformed volume. Stage V is transcendental stage of stamp sliding along the formed plane of failure. This stage did not reach in samples deformed by weak machine, but some rigid loading can be observed.

Frontal plane of stamp (1a) first shortly shifts down and then starts to rise (14 in Fig. 4b). Backplane (1b) shifts downward during stages I and II of the deformation (15 in Fig. 4b), and then starts to rise during stages III and IV.

The ultrasonic probes were located within drill holes (2) in central vertical stamp plane. One of the 3 zondes was always located near the front plane and the second one was near the back plane (1b). The third probe was utilized for ultrasonic tomography between the drilled holes. Such scheme permitted studying the macrofracture forming zones at all loading level.

After T load increasing the displacements increased during 10–15 min up to a stable value and velocity of the longitudinal (Vp) and transversal (Vs) waves were measured within 10 cm zonde intervals and along all possible tomography rays (12). The acoustic emission sensor (4) was located within a short drill hole near the front or back planes as well as at the stamp center for studying the local microseismic activity.
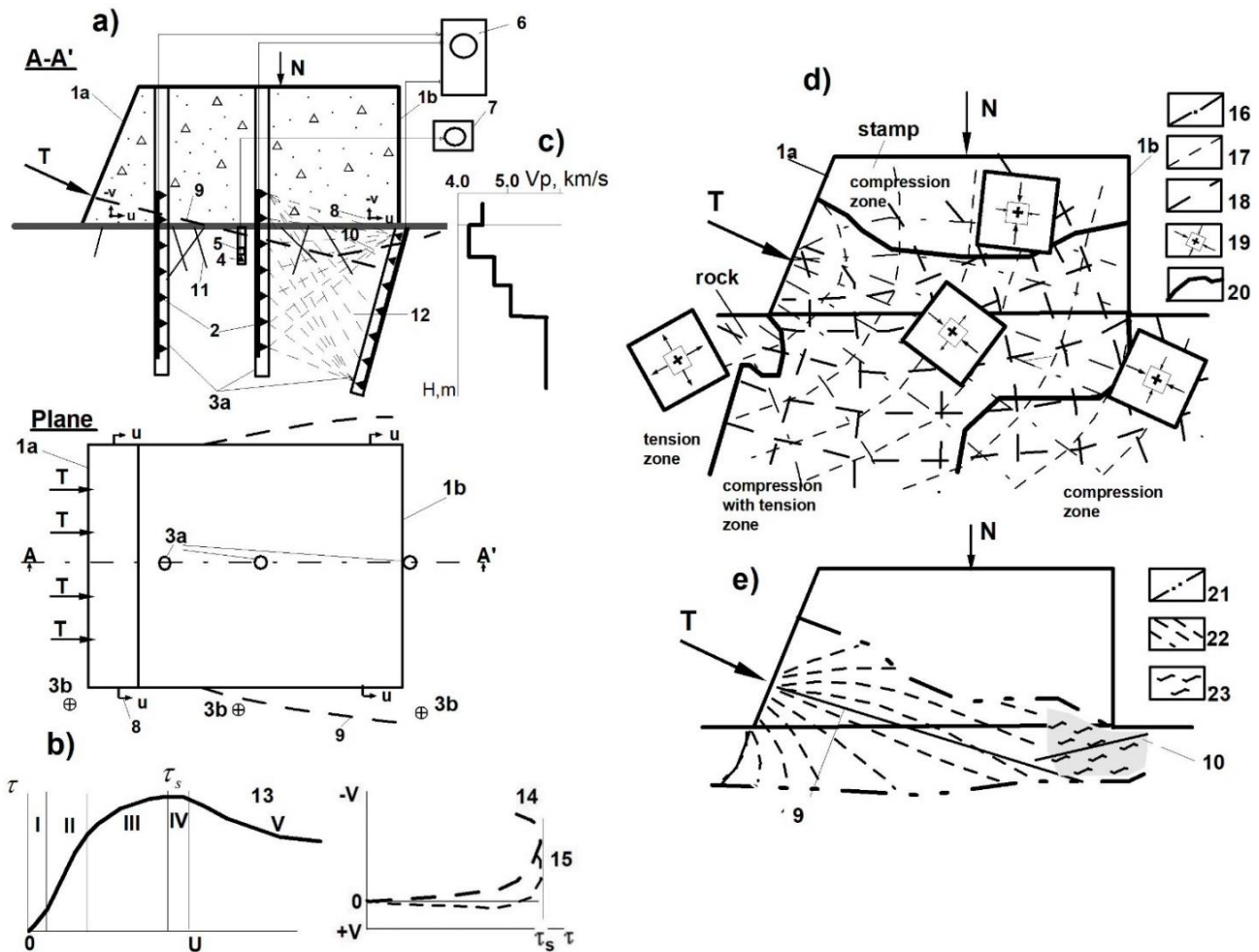
Fig. 4. General scheme of shear test. (a) Seismic-acoustic measurement layouts in section and in plane; (b) stamp total deformation (from left) and displacements of frontal and back planes (from right) graphs; I -V – stages of deformation; (c) typical velocity *Vp* graph in rock foundation; (d) Stress field; (e) plastic deformation area at the section of the 'stamp-rock' system at the load level of 0.85 from strength. Digits denote: 1a and 1b – front and back plains of stamp, respectively, 2 – US zonde, 3a – drill holes for US zonde, 3b – the same for AE sensor, 4 – AE sensor, 5 – preamplifier, 6 – US meter, 7 – magnetic tape, 8 – displacement meter, 9 – tensile macrofracture, 10 – shear macrofracture, 11 – natural joints, 12 – tomography rays, 13 – total stamp deformation, 14 – displacement of frontal (loaded) plane of the concrete stamp (1a) and 15 – the same of the back plane (1b), 16 –18 - traces of the main stresses σ_1, σ_3 and τ_{max} respectively, 19 – stress state mode, 20 – boundary of the different stress state mode zones, 21 – plastic zone boundary, 22 & 23 – rupture and shear microfractures, respectively.

4.1.2 Failure mechanism of the "stamp-foundation" system

The failure of "stamp-rock foundation" system (Fishman and Gaziev 1974) took place by tensile fracture at the frontal stamp plane (9 in Fig. 4d) and shear fracture or crushing (in the strongly heterogeneous rock) at the back one (10 in Fig. 4d). In the first case, the angle between the displacement vector and fracture plane was 60–90°and in the second case was30–45°. The foundation was stiff, the tensile character of fracture under frontal plane is clearly expressed. The typical macrofracture mode is represented in Fig. 4d. The failure started at the front (loaded) plane and the rupture fracture (9) was extended under the back plane. The final failure took place along shear fracture (10) at the back plane. The stress state at the "stamp-rock foundation" system is shown in Fig.

4c. The calculations show that the "pressure-tension" stress zone under the front plane and the "pressure-pressure" stress zone under the backplane were formed at the first load step. In accordance with Mohr criterion (Hoek 1968) the plastic zone was formed at the front plane and extended under back plane. At the loading level of 0.85 from strength the plastic zone occupies the all contact zone (Fig. 4d). One can see that the microfractures of the tensile mode were formed within almost all contact area apart from a small zone located near the back plane where shear microfractures were formed (10 in Fig. 4d).

4.1.3 Ultrasonic logging and tomography

The ultrasonic measurements were carried out using ultrasonic profiling inside boreholes (Ezersky and Goretsky 2014). The 7-element ultrasonic probes with distance

between sensors of 0.1 m were fixed within observation boreholes, which after mounting were filled with clay. The measurement lay-outs are presented in Fig. 4a. Ultrasonic profiling in boreholes is aimed to measure the distribution of *Vp* and *Vs* with depth.

Method and equipment. In ultrasonic logging (USL) the elastic waves propagate from a high frequency (50–70 kHz) transmitter to receivers along the borehole wall under investigation (Beck 1981). Savich et al (1969) suggested "dotty" (detailed) ultrasonic logging for measuring elastic velocities within 0.1–0.2 m distance along the borehole walls. Since the probe is held against the side of the wall, the results are unaffected by the "adjacent beds" effect (as it is in the seismic refraction method) because of the wave's direct path. Wave penetration into the rock is approximately 0.1–0.2 m in accordance to the wave length. The US-meter is intended mainly for ultrasonic measurements in boreholes using special multi-channel probe. The scheme of the dotted ultrasonic logging is shown in Fig. 5(a–c).

In our investigation, a 7-transducer probe (developed by Hydroproject Institute, Moscow, Russia), with a 0.1 m separation between the sensors (Fig. 5c), was placed into the borehole (Fig. 5a) and clamped onto the wall by means of a pneumatic camera pumped by air from the surface. It provided an excellent contact between the probe and the borehole wall. Every transducer (made of 70 kHz frequency piezoelectric ceramic) can act both as transmitter (T) and as receiver (R) when transducer is connected to generator or oscilloscope. Switching is performed with a switch-box (Fig. 5b). Elastic wave propagation along the borehole wall from transmitter arrives consequently to the receiving sensors where it is converted, gained, and visualized on the oscilloscope's electronic tube of the US-meter S-70 (Fig. 5b) that was described above.
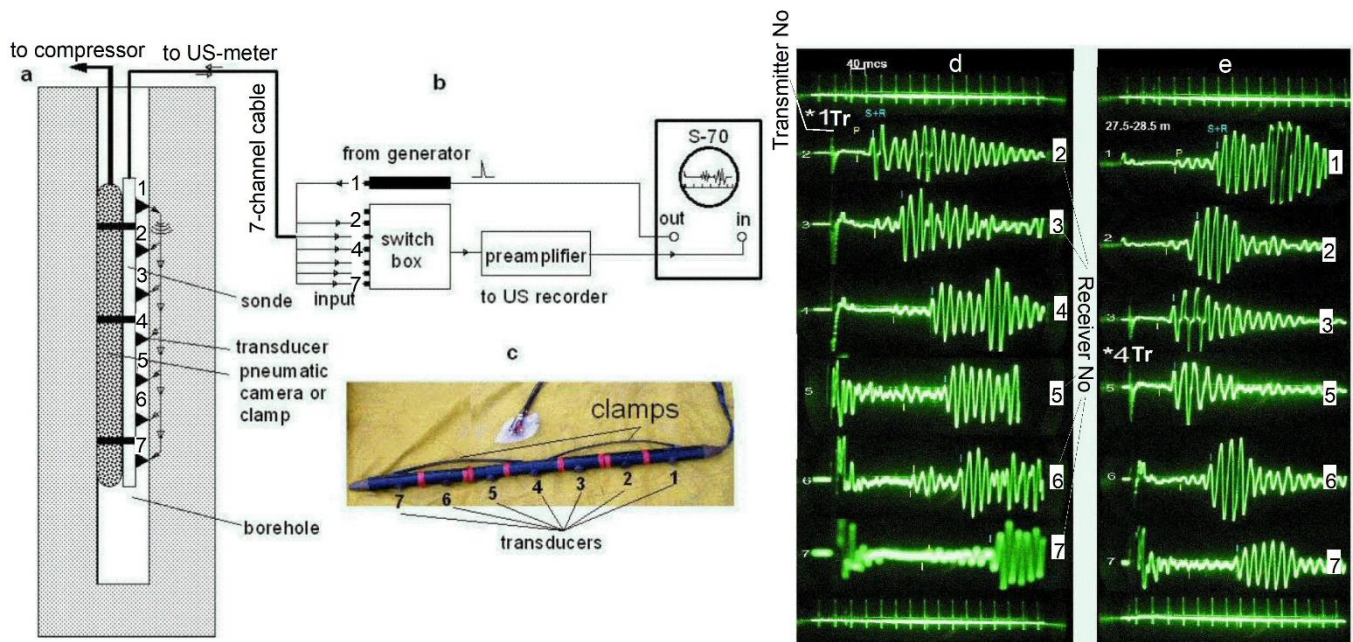
Fig. 5. Borehole logging lay-outs. (a) Ultrasonic logging: 7-transducer probe within the boreholes; (b) communication schema; (c) probe photography; (d, e) Ultrasonic records obtained during ultrasonic logging in the borehole (digits denote numbers of transducers); (d) 1st transducer is transmitter; 2nd to 7th transducers are receivers (direct shot); (e) 4th transducer is transmitter, the 1st to 3rd and 5th to 7th ones are receivers (split shot). *P* and *S + R* (interference shear and surface waves) arrivals are marked by green and white colors, respectively (Permission of Elsevier, Ezersky and Goretsky 2014).

There was also the moment of wave triggering (start of transmission) on the tube (see Fig. 5d). The time difference (*t*) between the triggering time and signal arrival at the nth receiver is the spread-time between transmitter and receiver along a fixed distance equal to the $l = (n - 1) \times 0.1$ m (the separation) between the neighboring sensors. The wave velocity is then defined by simply dividing: $V = l/t$. Examples of field records are presented in Fig. 5d & e. The transmitting transducer in Fig. 5d is No. 1 marked on records by an asterisk (see ultrasonic probe in Fig. 5c for explanation).

Figure 5e shows the records of ultrasonic pulses registered at receivers 2 through 6. Arrival times of *P*-waves are denoted by white vertical markers. Arrival times of *S + R*

waves are marked by green vertical markers. In Fig. 5e, the scheme of shot (named split) has been shown: the transmitter is transducer no. 4 and receiving transducers are 1st to 3rd and 5th to 7th. Physically, arrival times are calculated using a time scale (from above and below records). The time scale between two marks in Fig. 5d & e is 40 μs.

4.1.4 Acoustic emission measurements

In the acoustic emission method, elastic impulses are recorded that occur in a naturally stressed rock mass in the zones of formation and development of fractures termed as acoustic emission sources. These impulses as elastic waves propagate in the medium and reach the surface of the rock

mass (walls of excavation or boreholes, exposures, short holes, etc.) are recorded by acoustic emission sensors (Savich and Kujundjich 1990). During our studies response parameters were: $\dot{N}$ – acoustic emission intensity determined as a number of pulses in a unit of time (minute), N – total acoustic-emission or total number of impulses for a time interval of recording.

At AE measurements during stamp loading, AE sensor (4 in Fig. 4) was placed into a short hole (0.5 m depth) located at frontal (loaded), central or back planes (3b in Fig. 4) equipped by preamplifier (5 in Fig. 4). Impulses were recorded using a wide frequency range magnetic tape (7 in Fig. 4).

4.1.5 Some theoretical investigation of the microfault generation

Investigation of mountainous rock destruction is one of the most important problems of engineering geophysics. Solving the mentioned problems is impossible without careful studying of mountainous rock stability (Aleinikov 1999). It was considered earlier that destruction of some material was taking place when at least one component of the stress tensor reaches some critical value called as a "material durability". However, conducted analysis allowed us to conclude that such a notion is correct only for a relatively short-term action and is unsuitable for a prolonged stress to geological body or artificial object. Instead the notion "durability" was suggested to use the notion "longevity". On the basis of detailed theoretical analysis, we propose a new physical-mathematical conception describing the destruction process as a phase transition (Aleinikov et al 2000). From this point of view, generation of microfault (occurrence of empty space with maximal stress concentration) is an initiation of a new phase. Development of such a new conception permits us to recognize new relations between the destruction process on the one hand, and time, strength, temperature, pressure and characteristics of crystal lattice of mountainous rock on the other hand.

It was determined that microfault generation causes emission of a definite number of seismic-acoustical impulses (AE). Quantity of the impulses during a unit of time determines an intensity of the destruction process and frequency of oscillation indicates dimension of the microfault forming. It was proposed that a global changing of geological rocks under the effect of different physical factors may be also analyzed using the common approach considering the process as a phase transition.

For the common description of AE nature, it is necessary to apply all set of dynamic equations describing processes in heterogeneous medium (Aleinikov et al 2000).

The suggested conception makes possible procedures of long-term monitoring for different artificial underground constructions: buildings, mines and reservoirs as well as other artificial and natural structures that are for forecasting potential seismological events.

4.2 Results of large scale tests

4.2.1 Behavior of Vp during stamp loading in zones of two macrofracture types during stamp loading up to failure

The dimensional velocity variations at different distance from macrofracture of tensile or shear are shown in Fig. 6. The dependences for medium foundation stiffness are analyzed. The rupture zone is characterized by the gradual velocity decrease (Fig. 6a) at all stages of loading. The decrease amplitude ($\delta V\% < 0$) is maximum close to macrofracture position (-24 − -30%) and it decreases as distance from macrofracture increases (to -4%). In distance of 0.3–0.4 m velocity ($\delta V \%$) changes sign to positive.

In shear zone velocity behavior is more complex (Fig. 6b), but on the whole, it is quite regular. The common for all tests is existence of the depth interval (0.1–0.3 m), which demonstrates sharp velocity decrease from the first loading step. This decrease then is changed by the gradual velocity increase. This depth interval is located on continuation of the shear load line and is evidently connected with features of the loading geometry. Other regularity is a common velocity increase in all depth intervals up to loading level of 0.65–0.80 from strength. Then velocity decrease starts and continues to system failure.

The tomographic (circular) velocity variations with a stress level under back plane (zone of shear fracture forming) is shown in Fig. 6c. One can see that at $\tau = 0.5\,\tau_s$ (stress mode is pressure as 6d) velocity increases in all directions up to 5–10% of that at $\tau = 0$. Then, at $\tau = 0.86\,\tau_s$ (stress mode is pressure with tensile as 6e) circular diagram shows velocity decrease in directions of tensile stresses.

Note that in all cases the system failure took place at the background of the velocity decrease. This decrease started at the lower load level (0.65–0.8 from ultimate load) for weak rocks and at the load level of 0.9 was more for stiff rock foundation. The integrated velocity decreases in shear zone before the system failure was 8–12% on average (Fig. 6b & c). Thus, the character of the velocity behavior is defined by the macrofracture mode that in its turn is defined by stress mode. The velocity variation amplitude depends on stress-state mode, normal stress level and the primary (before loading) rock elastic properties.

4.2.2 Active zone

Analysis of the velocity behavior at the different distances from macrofracture zone has shown that it is complex and difficult to define the deformation stage using interval velocity only. The above results show that in real rock mass the main deformations are localized within zone (named active zone), which is characterized by heightened velocity and geomechanical parameter variations. It could be supposed that integral characteristics of this zone completely reflect deformation process, which are not homogeneous within this zone. It was established using statistical analysis that the active zone sizes in rupture zone is 0.3–0.4 m (or 30–40% of the stamp size) and in shear zone is 0.5 m (or 50% of the stamp size).

In Fig. 7a & b active zone velocities variations V_{av} are represented as again loading level. One can see that active zone integral velocity graphs are similar to generalized velocity behavior of samples during the deformation process preceding tensile (a) and shear (b) failure (see Ezersky 2017, Fig. 7c). Velocity variations δV from V_{av} derived from

different tests are shown in Fig. 7c by horizontal bars.

Specific feature of this study is a selection of the observation technique which allows velocity measuring along minimum normal stress direction. The numerous studies of samples failure have shown that this measurement direction is more informative at the inelastic deformation and failure stage. In all testes, the "stamp-rock" system failure took place at the velocity decrease connected with microfractures tensile (5 in Fig. 7c) and shear (6 in Fig. 7c) forming. Velocity variation took place during system failure at the removal of 0.3–0.4 m from macrofracture for both tensile and shear zones (curve 3 in Fig. 7c). Comparison of velocity variation at stresses close to failure and after failure (curves 1 and 2 in Fig. 7c) shows that they are different. Distribution of V_{av} in the tensile zone under frontal plane is the same as before failure, whereas distribution of V_{av} in the shear zone (under back plane) shows a great difference in the frames of active zone: V_{av} does not return to pre-failure values manifesting on residual deformation within the zone of shear failure. The work conducted by Ezersky (2017, Fig. 10c & d) has shown similar regularities of V_{av} variation in active zone during 2 cycles of loading. He suggested that the tensile microfractures in the tensile failure zone are completely closed after unloading the system. In the shear failure zone (under back plane) velocities are not restored after stamp unloading. It indicates that there are formed shear

microfractures, which cannot restore shape because of the friction. The interaction between these fractures evidently takes place that also counteracts to microfractures closing and velocity restoration.

Evidently, macrofracture forming results in the rock unloading and microfractures closing out of the failure zone. The results show that within failure forming zone the complex velocity variation takes place (especially in the stiff rock). It is connected with a heterogeneous rock structure, loading geometry as well as stress redistribution after local fracture forming within deformed volume. At the same time velocities measured in the active zone clearly reflect the deformation process stages and its difference within rupture and shear failure zone. The material compaction is accompanied by the velocity dispersion decrease. Contrarily, the material failure, leads to velocity decrease. Velocity dispersion within failure zone increases. Analogues results were obtained in the Inguri Dam long-term monitoring (Savich et al 1983).

4.2.3 Regularities of AE in vicinity of tensile and shear macrofractures

Deforming of stamp is accompanied by the AE triggering. Let us consider regularities of AE in every of the tensile and shear zones (Fig. 8). To determine AE in zones of different fractures, AE sensor was placed in different holes located
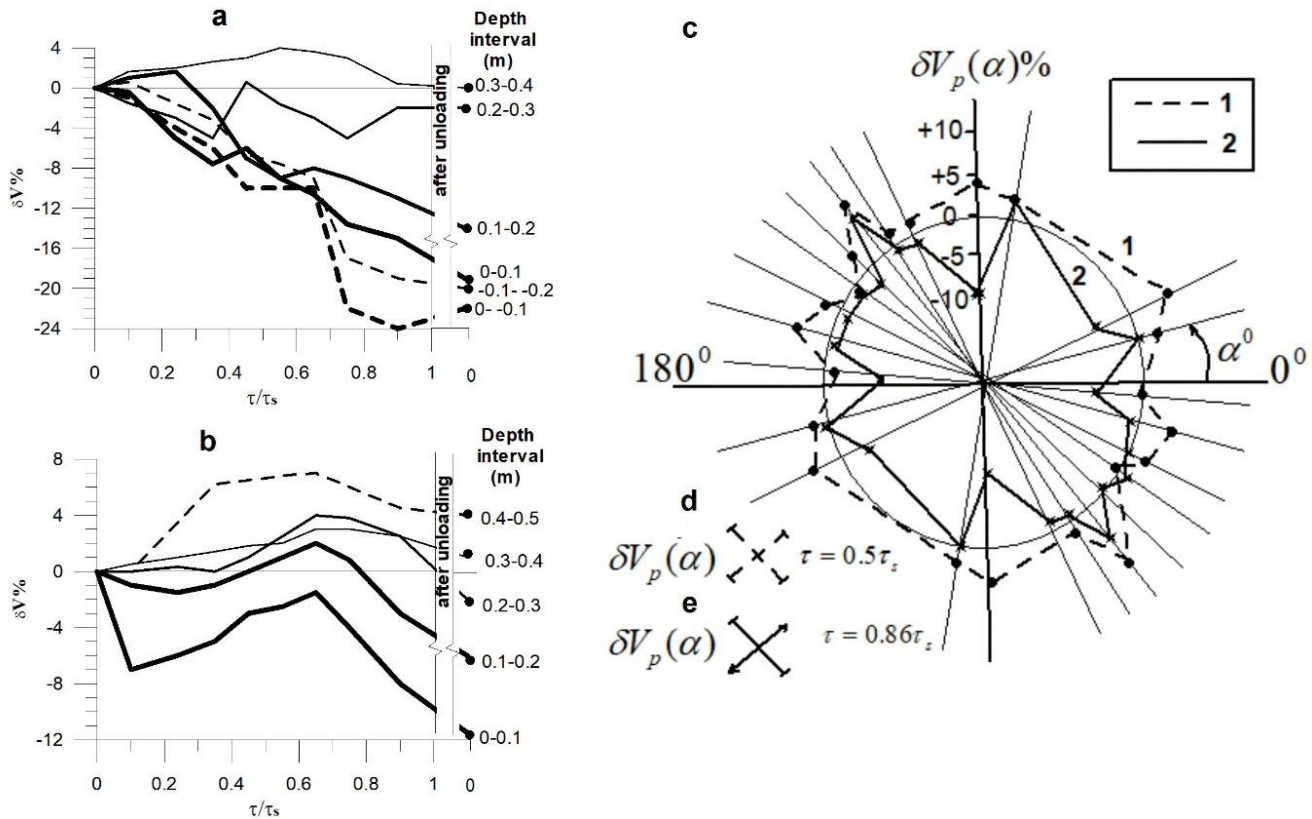
Fig. 6. Relative interval velocity variations δV% vs relative shear stress τ/τ_s graphs: (a) in a zone of the rupture macrofracture (under frontal plane); (b) in a shear fracture zones (under back plane); (c) tomographic (circular) velocity variations with a stress level; 1 – velocity diagram at $\tau = 0.5\tau_s$ (stress mode is pressure as (d)); 2 – at $\tau = 0.86\tau_s$ (stress mode is tensile with compression as (e)). H/B – is depth to stamp size Ratio.
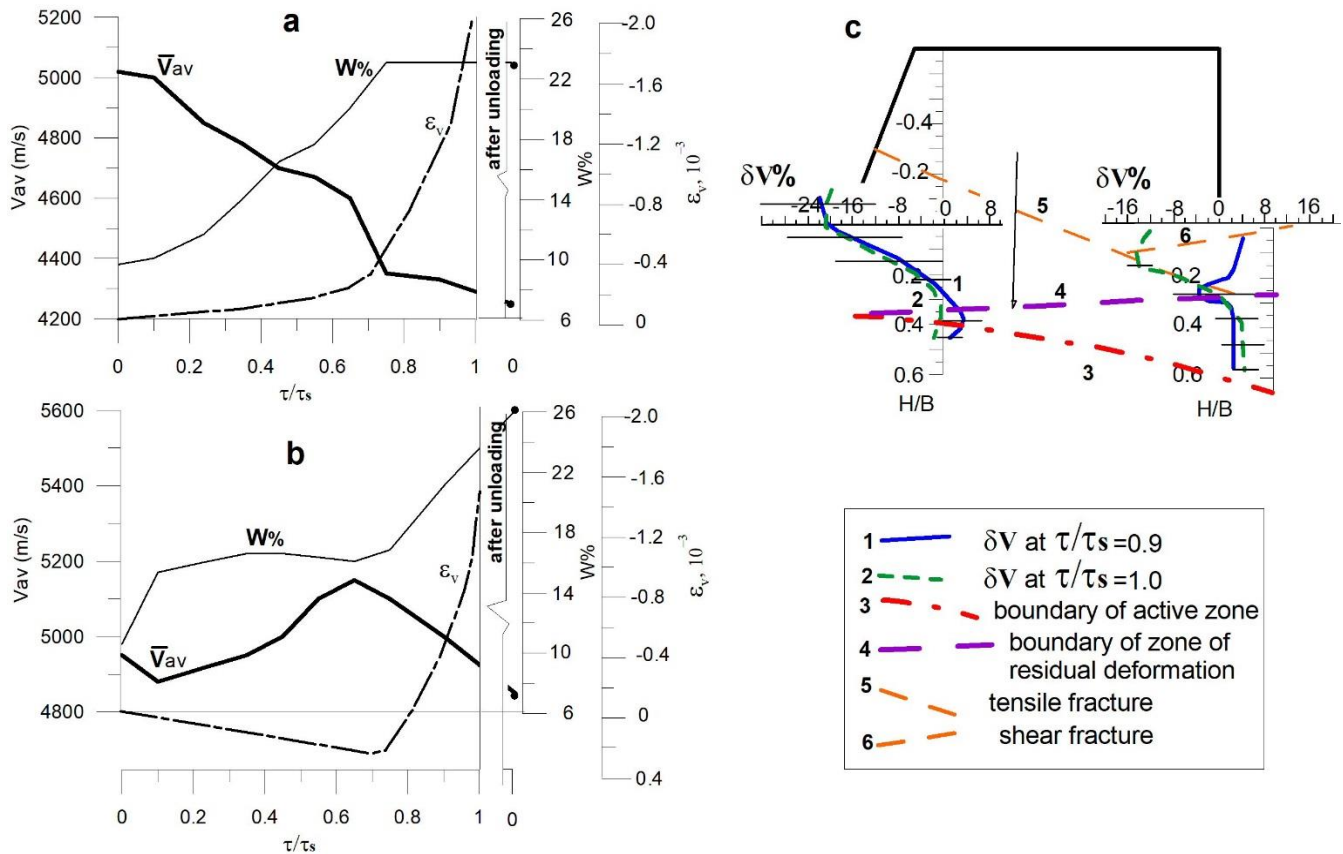
Fig. 7. Variations with loading level of active zone velocity $\bar{V}_{av}$, variation coefficient W% and summary active zone vertical deformation ε_v in the tensile zone (a) and shear failure zone (b); (c) distribution of average velocity variations under the frontal (loaded) stamp plane and back one at load level $\tau/\tau_s = 0.9$ (1) and after failure (2). Horizontal bars characterize velocity variations δV from V_{av} during different tests.

either close to frontal or back planes (3b in Fig. 4a). *In the tensile zone* (Figs 8a–c) appearance of AE pulses is connected with starting of the frontal plane rise and continues during all loading gradually increasing. AE is raised by groups, including some impulses.

However, some notable increase of energy of single pulse is observed at $\tau/\tau_s = 0.53$. Power of AE, calculated as sum of energy of pulses per minute, rises by order before failure. This clearly determines approach of failure (Fig. 8b).

During shear failure, AE sensor was placed close to back plane (shear failure). Here impulses start to appear at more loads $\tau/\tau_s = 0.8$ (Fig. 8d–e). Impulses have more amplitude, but are emitted rarer. A more distinct difference is observed at comparison of accumulative acoustic emission (Fig. 8g). At tensile fracture forming (curve A) increase of AE is more significant than in the case of shear fracture (curve B). In case B sharp accretion of AE activity starts at $\tau/\tau_s = 0.9$–0.95.

5 Case Histories

The Zhinvali project on the Aragvi river (Georgia) was designed for electricity generation, water supply to the city of Tbilisi (capital of Georgia) and irrigation of surrounding agricultural lands (Fig. 9).

Serious complications during construction were caused by driving of the tailrace tunnel where a number of geophysical methods were used enabling the following engineering problems to be resolved: additional study of engineering geological conditions, forecast of rock pressure on the lining (Ezersky et al 1991b, 1993a, Rudyak 1996), and monitoring of rock pressure development in the process of mining.

At the stage of tunnel construction, numerous ultrasonic surveys in the anchor boreholes were carried out. Statistical estimations of the forming and structure of the unloading zones were performed. Later during the tunnel excavation, a monitoring network was employed which covered engineering-geological, geophysical (ultrasonic and acoustic-emission), and dynamo-deformometric observations. It gave a chance to observe at the same time the unloading zones development connected with the construction works (Ezersky et al 1991b, 1993a). In this work, the main attention is spared to analyze the stabilization of pressure to lining based on integrated geophysical monitoring.

Twenty years after the Project completion, validity of conducted investigation is confirmed, and it was proposed to describe in detail an experience of geophysical methods application.
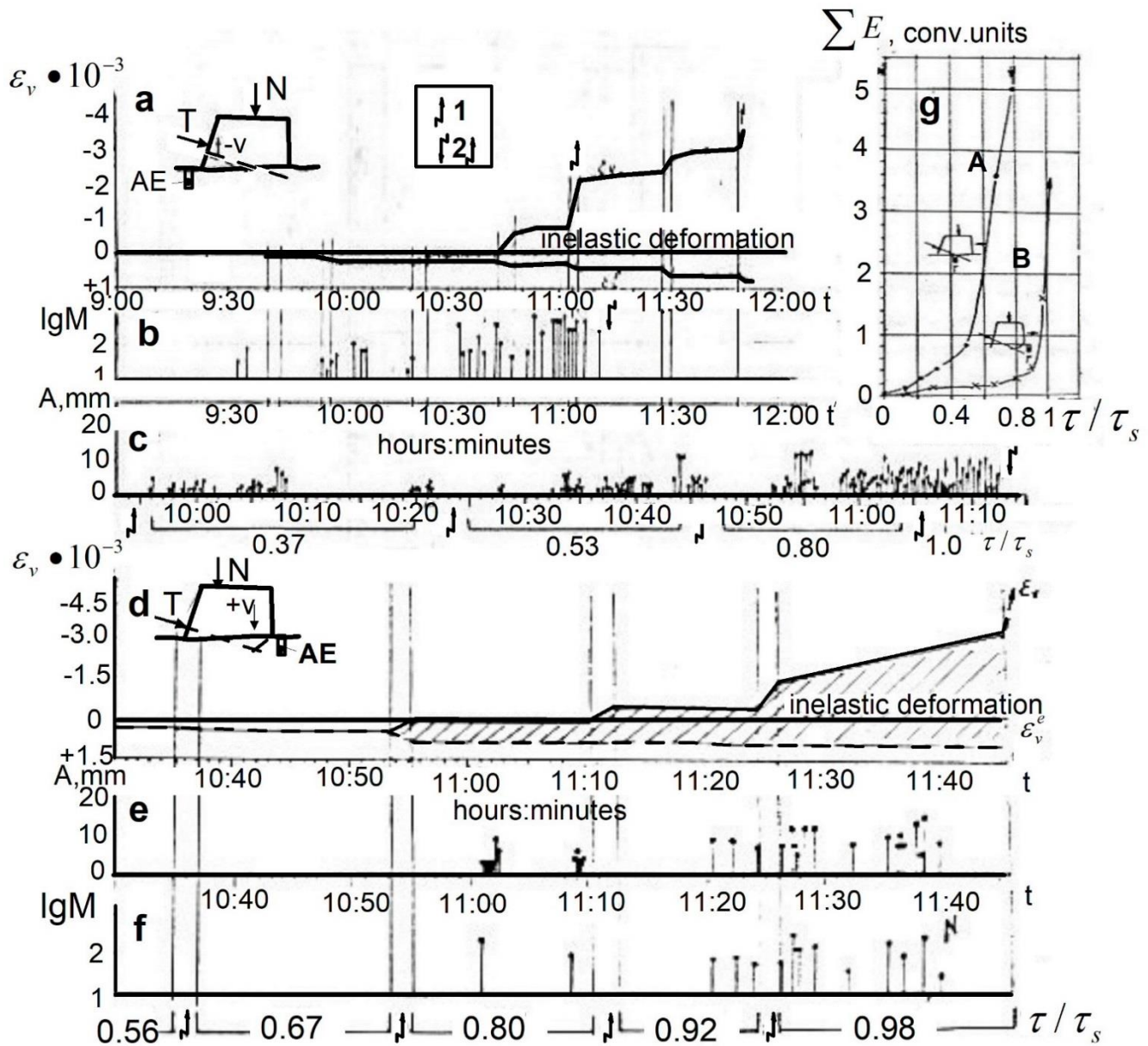
Fig. 8. Acoustic emission (AE) in zones of tensile and shear macrofracture formation under shear loading. (a–c) deformations of stamp, acoustic energy and amplitude of AE, respectively, versus time and relative shear stress; (d–f) deformations of stamp, amplitude and acoustic energy of AE, respectively, versus time and relative shear stress; (g) total acoustic energy ΣE (in conventional units) versus shear stress during formation of tensile (A) and shear (B) macrofracture. 1 – increase of stress, 2 – finish of AE registration.

Fig. 9. Zhinvali Project in Georgia (Left – European countries, right – Georgia map). 1 – Location of Zhinvali HPS.
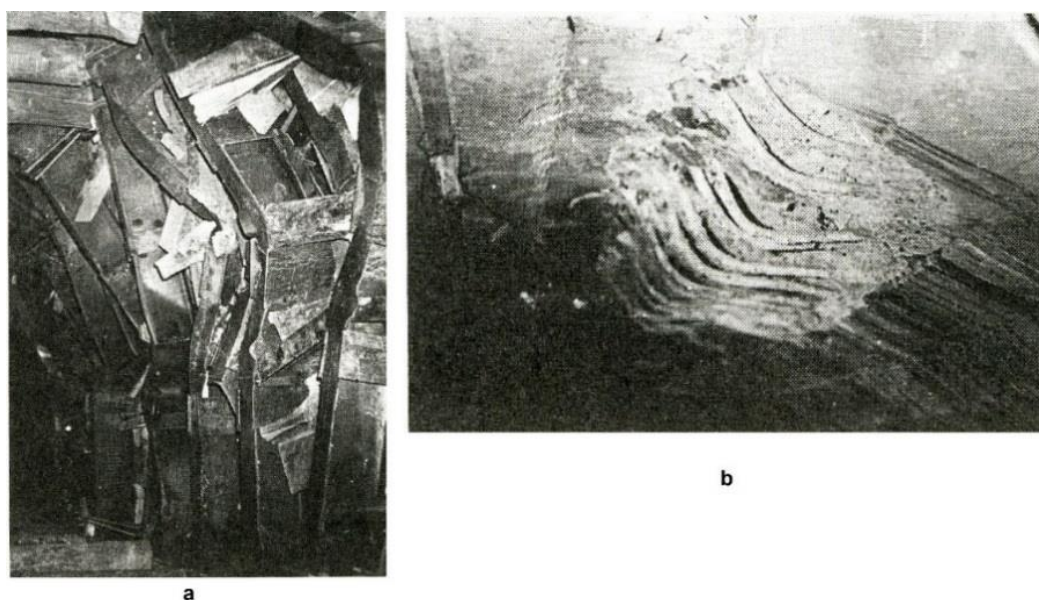
Fig. 10. Example of failure of arch still support (a) and temporary lining (b) in the second working face (Author's photograph).

The section of the tailrace tunnel of the Zhinvali Project between the working faces No.1 and 2 was driven in the argillaceous rocks of the Upper Eocene represented by argillaceous clays and clay shales with interbeds of thin laminated sandstones. The argillaceous rock strata are characterized by complex intensive tectonics, rocks contained gaseous components and both working faces occurred in the gas conditions. In the course of driving of the tunnel at the section of clay shales and argillaceous clays, intensive manifestation of rock pressure began in the form of deformation of an arch still support, squeezing of reinforcing in the concrete and lining and rockfall (Fig. 10). Ten-twelve days after driving, first indicators were observed and later pressure rose during 2–3 months, and sometimes 6 months up to 0.5–0.6 MPa which resulted in convergence of tunnel walls to 0.8 m. The failure of the lining and rockfall occurred at different distances from the working face and consequently the rate of mining decreased from 30 to 10 m/month.

Seismic and electric methods (carried out at the earth's surface) enable us to define more exactly the engineering-geological structure and physical-mechanical properties of rock in the unfinished section of the tunnel (Fig. 11). According to geophysical investigations, the zones of rocks of different lithological types and degrees of weathering were singled out in the cross-section of the tunnel, inclinations of boundaries between these zones, which were extrapolated to the depth of the tunnel location, were determined. Two large zones of weakness associated with the extensive crush with thickness of zones up to 400 m were confirmed later by the data of satellite surveying (Mastitsky and Kereselidze 1989).

Apart from two tectonic zones where two benches of rocks were identified as unweathered clay shales and argillaceous clays with low elastic and strength characteristics, argillaceous sandstones characterized by higher elastic properties were distinguished in the section.

The following tasks were emphasized for the further of geophysical investigations:

- Revealing the nature of higher rock pressure on the lining;

- Evaluation of rock pressure on lining at the already driven section of the tunnel (in comparison with the data of direct measurements);

- Forecast of possible values of rock pressure at unfinished sections of the tunnel route;

- Set up of routine monitoring of rock pressure development in the process of mining.

For solution of the abovementioned problems the authors of the paper developed the procedures and integrative package of geophysical methods which became an integral part of the mining process including elements of the "New Austrian tunneling method" such as guniting, anchoring of rocks, monitoring of deformation development of the rock mass and the lining as well as correction of the anchoring parameters.

Ultrasonic and acoustic emission methods were used for monitoring of tunnel stability (Savich and Kujundjich 1990) that have been described above (sections 4.1.3 and 4.1.4).

As it is shown above (section 4), on the basis of analysis of experimental and theoretic works (Hardy et al 1969, Vinogradov et al 1975, Savich and Kujundjich 1990, Aleinikov et al 1999, 2000, Ezersky 2017) acoustic emission intensity generated by stressed volume of the medium is determined by the level of shear stresses (τ/τ_s, where τ_s is shear strength); it is in proportion to the rate of deformation of the volume ($\dot{\varepsilon}$) and for particular types of rocks and conditions of deformation it may serve as a measure for both. The value of total emission N is in proportion to complete deformation of considered volume of the medium for the period of recording. These regularities themselves were observed in different scales of studies and for a wide range of rocks and concretes. A combination of ultrasonic and acoustic emission was utilized to reveal the nature of failure
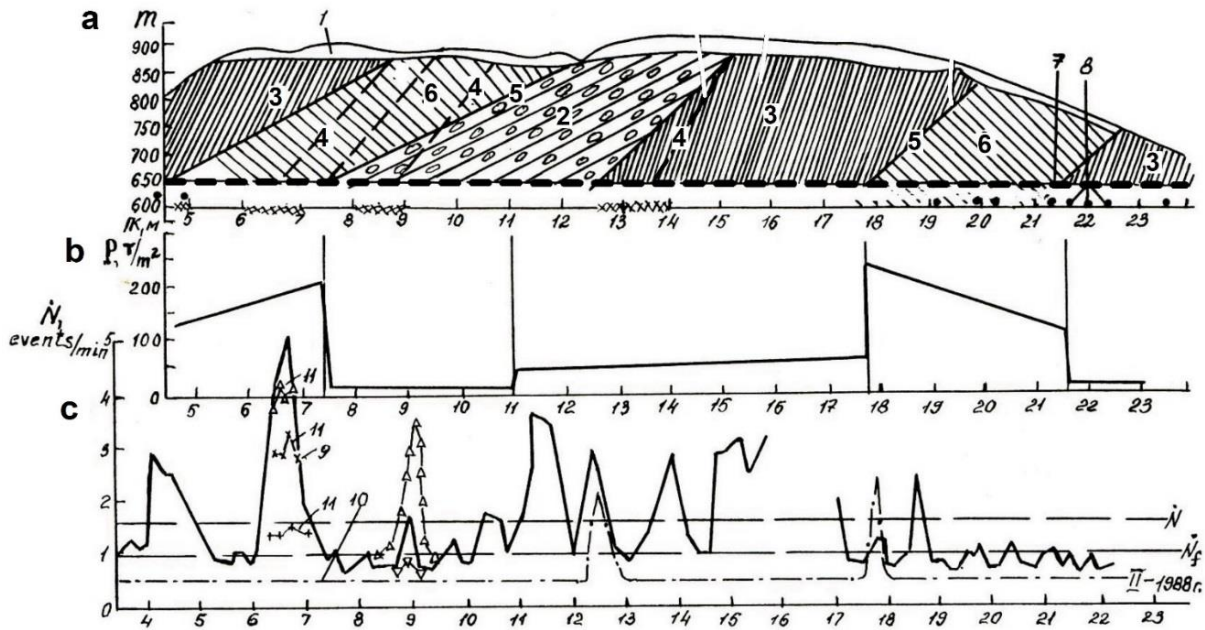
Fig. 11. Geophysical forecast and monitoring of rock pressure at the tunnel route. (a) geological section along the tunnel trace; (b) pressure diagrams of forecasted rock pressure (after Ezersky et al 1993a); (c) diagram of acoustic emission intensity in lining in different periods. $\dot{N}_f$ – background intensity of AE. 1 – Quaternary deposits; 2 – argillaceous sandstone; 3 – clay shale and argillaceous clays, 4 – alternative boundaries, 5 – boundaries of zones of different lithology and degree of weathering, 6 – zones of tectonic dislocation, 7 – tunnel route, 8 – points of ultrasonic observations, 9 & 10 – curves of $\dot{N}$ in different periods of construction and exploitation, 11 – intermediate examination of anomalous sections.

and higher pressure on the lining. For this purpose, fans of boreholes were drilled at different stations of the tunnel in zones of different manifestation of pressure where ultrasonic and acoustic emission studies were carried out. Typical curves of distribution of values Vp and $\dot{N}$ along the boreholes are shown in Fig. 12.

Variation curve $Vp = f(h)$ (Fig. 12a) points to occurrence of zone of weak rocks of 4–5 m in thickness in this specific case. At the same time, on the curve $\dot{N} = f(h)$ (Fig. 12b) within the zone of weakness a higher level of $\dot{N}$ (compared with deep portions of the rock masses, where $\dot{N} = \dot{N}_f$) is observed, and in this case the curve has a well-defined maximum of intensity $\dot{N}_m$ at a depth of 1.0–3.0 m.

Similar results allow us to draw a conclusion that a basis of higher rock pressure on the lining is formed by process of rock cracking which causes dilatancy of the rock mass and consequently intensive displacement of the contour inside the excavation. The form of distribution of parameter $\dot{N}$ with depth points to plasto-elastic nature of the field stresses. It should be noted that maximum of curves $Vp = f(h)$ and $\dot{N} = f(h)$ do not coincide that is probably connected not only with the distribution of stresses, but with strength properties of rocks and different type of stress state.

Routine observations (monitoring) at equipped fans of boreholes demonstrated that stress-relief of the rock mass takes place during a long period of time and at unstable section stabilization is not detected after several years. Study of distribution of wave velocities and AE intensity in the rock masses demonstrated that the nature of stress-relief and

interaction of the rock mass and the tunnel lining vary with time depending on bearing capacity and state of support. At the unstable sections, sizes and configuration of unloading zone depend on a state of the lining: a flexible lining favours enlargement of thickness of the decompaction zone (more than 10 m) (Fig. 12d), whereas, a more rigid lining decreases the size of the decompaction zone to 5–8 m (Fig. 12e). At stable sections, the formation of the unloading zone and attaining of equilibrium in the "support-rock mass" system take place mainly during 2–3 months. At these sections distribution of Vp and $\dot{N}$ have the form shown in Fig. 12a & b. Another important conclusion is drawn from a circular configuration of velocity isolines (Fig. 12e) that points to a hydrostatic nature of stress field in a plane normal to the axis of the tunnel ($\sigma_1 = \sigma_3$) (complicated by fracturity) and, consequently, stresses in a rock mass are assessed by value $\sigma_1 = \gamma H$ varying from 2.5 to 5.0 MPa according to the depth of tunnel location.

In Fig. 13a & b velocity of displacement of temporary support $\dot{u}_r$ and their absolute values u_r are compared with curves of AE intensity $\dot{N}$ and total AE N. The comparison indicates that temporary relationships of acoustic parameters are similar to corresponding curves $\dot{u}_r = f(t)$ and $u_r = f(t)$ typical of the stable interacting system "rock mass-lining".

For analysis values $\dot{N}$ at $t > t_0$ were used where $t_0 = 2$–3 months. In the process of tunnel excavation, supporting and holding for 2–3 months measurements of acoustic emission intensity in the concrete lining were taken along the whole

driven length in conformity with the developed procedure. On the basis of measurement, diagram of distribution $\dot{N}$ along the axis of the tunnel (Fig. 11c) was generated where

the strength of experimentally determined AE criteria of hazardous zone stability with respect to failure of the lining was distinguished.
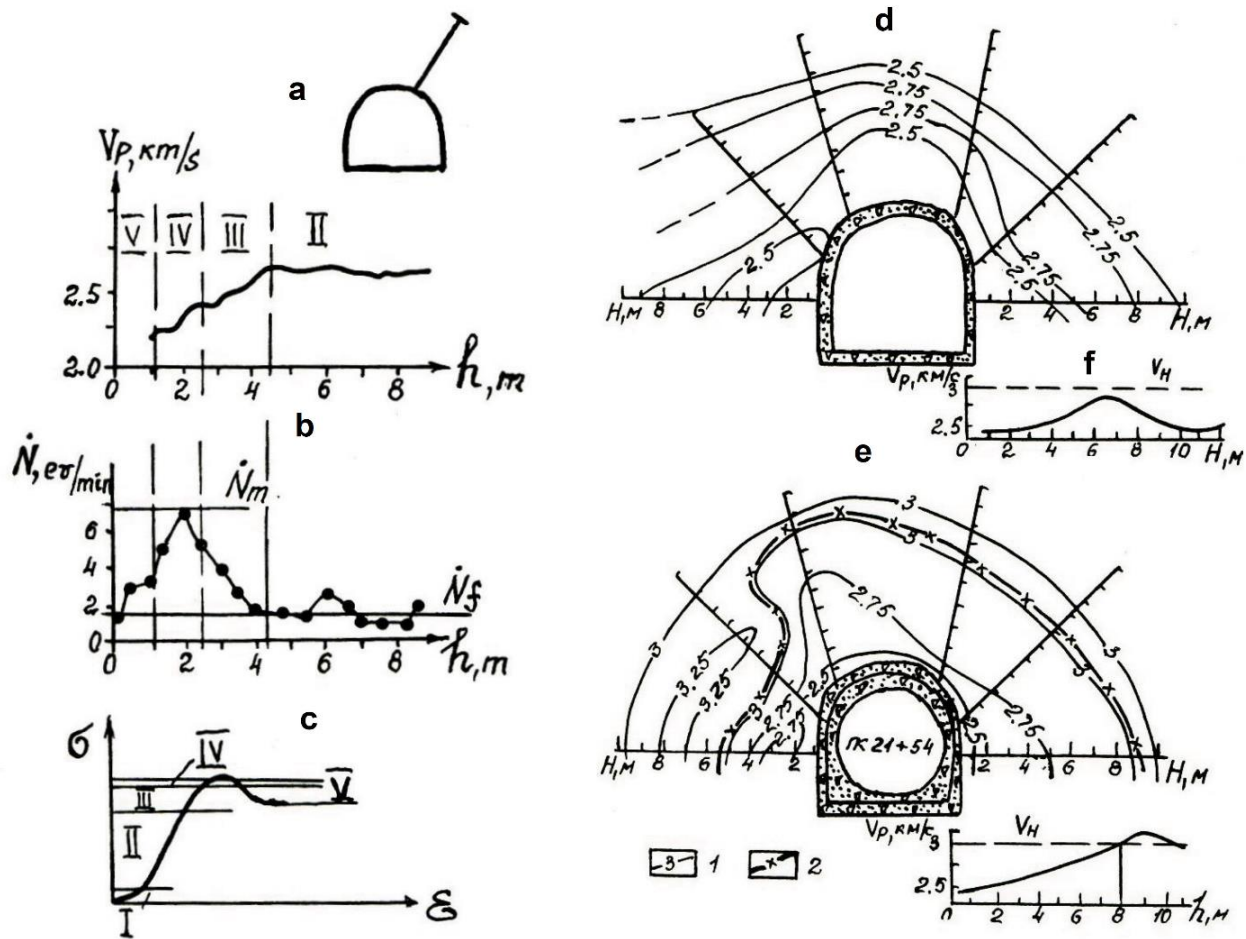
Fig. 12. (a) Distribution of Vp along borehole; (b) intensity of AE $\dot{N}$ ($\dot{N}_m$ – maximum value by borehole; $\dot{N}_f$ – background AE intensity); (c) stages of stress-strain state according to Pacher (1970): I – inelastic; II – quasi-elastic; III – plasto-elastic; IV – failure; V – plastic deformation; (d–f) effect of lining reinforcement on distribution of wave velocity Vp in section of tunnel driven in argillaceous rocks according to data of ultrasonic investigation: (d) with damaged lining; € ditto with reinforced lining; (f) curves of velocity variation along borehole; 1 – velocity isolines Vp, km/s; 2 – boundaries of unloading zone.
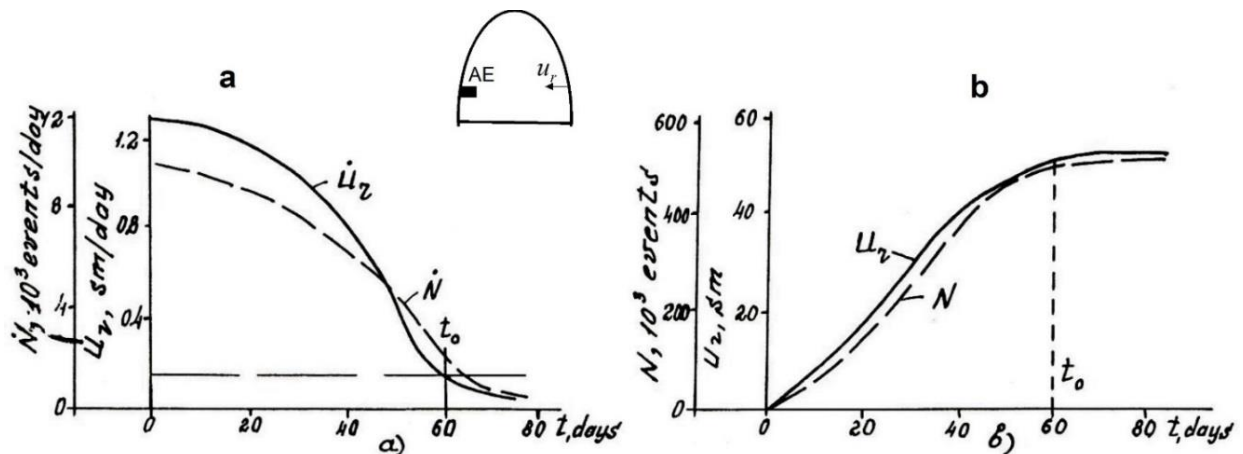
Fig. 13. (a) Curves of temporal variation of rate of displacement of contour of tunnel lining $\dot{u}_r$ and AE intensity $\dot{N}$; (b) values of displacement u_r and total AE N: AE – pickup of acoustic emission; u_r – displacement vector; t_0 – time of deformation stabilization.

In these zones strengthening measures were taken to stabilize deformations of the rock mass and the lining. These measures included installation of anchors of different length (up to 10 m) and different combination and pattern and filling grouting as well. After strengthening repeated measurements of acoustic emission were taken and if necessarily, strengthening was repeated.

Thus, monitoring carried out in the tailrace tunnel of Zhinvali Hydropower station at sites of intensive rock pressure to lining, made it possible to obtain new data on time history of unloading of rocks, its relation to a stress-strain state, physical and mechanical properties of the rock mass, procedure of its supporting and rigidity of lining. A pattern of curves of spatial distribution of velocity of elastic waves *Vp* around the tunnel in conjunction intensity of AE represent distribution of stresses and strains near the tunnel opening. Distribution of these parameters in space and variability in time makes it possible to examine the nature of interaction of the rock mass and supports described by mechanical-mathematical models. For instance, in our case, a rigid support interacts with the medium according to the law described by a plasto-elastic heterogeneous model while a decrease in rigidity of the support (for instance, due to failure) results in a change of the nature of interaction described by a rigid-plastic model. The described results make it possible to use geophysical (in particular seismic-acoustic) methods both for the forecast of rock pressure at the stage of designing underground structures and for the flexible revision of mining procedures at the stage of construction.

6   Conclusions

1. The examples described above point to great potentialities of the geophysical methods for rock deformation monitoring. The velocity measurements allow us to understand the fracture parameter variations both in space and time. An important factor is correct measurement arrangement. The velocity measurement along major stress directions gives different information at different deformation stages. The active zone as a zone of the heightened deformation variation is the second important factor for monitoring deformation process.
2. For the planning of effective monitoring information, stress state and geometry of the stress field are required.
3. Monitoring carried out in the tailrace tunnel of Zhinvali Hydropower station (Georgia) at sites of intensive rock pressure to lining, made it possible to obtain new data on the time history of unloading rocks, its relation to a stress-strain state, physical and mechanical properties of the rock mass, procedure of its supporting and rigidity of lining.

Acknowledgements

References

Acrimony, J.A., J. Larsson, R. Reveler and P. Colin, 1987. Displacement Remote Monitoring and Seismic Acoustics: What is Best Fitted to the Monitoring of Rock Caverns. Proc. of the ISRM Int. Symp., Helsinky, 1986. Rotterdam, Balkema. p885 - 900.

Aleinikov, A.L., V.T. Belikov and L.V. Eppelbaum, 1999. Investigation of Rock Destruction: A Novel Physical-Mathematical Approach. Collection of Selected Papers of the SAGEEP-99 Confer., 12, Oakland, USA. p609 - 618.

Aleinikov, A.L., V.T. Belikov, L.V. Eppelbaum and N.I. Nemzorov, 2000. Mountainous rock destruction and metamorphic processes in the Earth: a view from classical physics. Scientific Israel, **3**: 65 - 87.

Barta, J., J. Jirků, D. Dostál, J. Kněz, L. Slavík and J. Vilhelm, 2014. Monitoring Chování Puklinových Systémů Horninového Masivu Geofyzikálními Metodami – Informace o Probíhajícím Ukolu TA 03020408. Hydrogeologická a Inženýrskogeologická conference. Liberec 2014.

Barta, J., D. Dostal, J. Jirku, V. Kopezki, V. Slavik and J. Vihelm, 2016. Long-term monitoring of rock mass properties in the underground excavation. Available at http://www.gimpuls.cz/17.pdf.

Beck, A.E., 1981. Physical Principles of Exploration Methods. Macmillan Press Ltd., London.

Brace, W.F., B.W. Poulding and C. Scholz, 1966. Dilatancy in the fracture of crystalline rock. J. Geophys. Res., **7**(**16**): 3939 - 3953.

Brady, B.T., 1974. Theory of earthquakes, 1. A scale independent theory of rock failure. Pure Appl. Geophys., **112**: 701.

Bulychev, N.S., 1982. Mechanika Podzemnyh Sooruzheniy. Textbook for high schools. Nedra Publishers, Moscow. p270.

Da Gama, C.D., 2004. A method for continuous monitoring of tunnel deformations during construction and service phases. EUROCK'2004, Salzburg, Austria. Available at http://cegeo.ist.utl.pt/html/investiga/met.pdf.

Drescher, K. and M.F. Handley, 2003. Aspects of time-dependent deformation in hard rock at great depth. The Journal of the South African Institute of Mining and Metallurgy, 325 - 335. Available at https://www.saimm.co.za/Journal/v103n05p325.pdf.

Ezersky, M.G., 1985. Seismic-acoustic Parameters Behavior Preceding to Samples and Rock Mass Failure. Ph.D. thesis, Moscow Institute of the Physics of Earth, the Russian Academy of Sciences. (in Russian)

Ezersky, M., 2017. Behavior of seismic-acoustic parameters during deforming and failure of rock samples, large blocks and underground opening - base for monitoring. International Journal of Geo-engineering, **8**(**13**): 1 - 19. doi: 10.1186/s40703-017-0050-2.

Ezersky, M.G. and I. Goretsky, 2014. Velocity-resistivity versus porosity-permeability inter-relations in Dead Sea salt samples. Engineering Geology, **184**: 96 - 115. doi: 10.1016/j.enggeo.2014.09.009.

Ezersky M.G. and I. Goretsky, 2015. The scale effect of Dead Sea salt velocities based on seismic-acoustic measurements. In: Roberts, L., K. Mellegard and F. Hansen (Eds.), Mechanical Behavior of Salt VIII, CRC Press. p137 - 144. doi: 10.1201/b18393.

Ezersky, M.G., M.M. Iliin, B.P. Yakovlev and A.V. Kolichko, 1991a. Specific of Rock Mass Unloading during Construction of the Rogun Hydropower Station with the Use of Geophysical data. Proc. of the 7th ISRM Intern. Congr., 1991. Aahen, Deutschland. p1099 - 1104.

Ezersky M.G., M.S. Rudyak and K.V. Kobaladze, 1991b. Monitoring Rock Pressure in the Discharge Tunnel at the Zhinvali Hydro-Power Station. Hydrotechnicheskoe Stroitelstvo, No.3, p24 - 27. (in Russian)

Ezersky, M.G., V.N. Zhukov and V.A. Jakubov, 1992. Geophysical Monitoring of "Rock Bolt/Rock Mass" System and its Variation with Time during Construction of Large Underground Works. Proceedings of ISRM International Symposium, Sudbury, Ontario, Canada. June 16–19, 1992. Balkema, Rotterdam, Brookfield. p245 - 253.

Ezersky, M.G., M.S. Rudyak and V.V. Zhdanov, 1993a. Forecast and Stability Monitoring of Zhinvali Project Tunnel on Basis Geophysical Data. Proceedings of ISRM International Symposium. Istanbul, Turkey. April 5–7, 1993. Balkema, Rotterdam, Brookfield. p485 - 491.

Ezersky, M.G., S.I. Skiba and A.D. Mikhailov,1993b. Geological Geophysical Monitoring of Stability of the Underground Power House of Hoabinh Project (Vietnam) during Construction. "Eurock'93", Lisboa, Portugal. Proceedings of ISRM International Symposium. June 21–24, 1993. Balkema, Rotterdam. p535 - 544. (also published in: Hydrotechnicheskoe Stroitelstvo, 1990, **5**: 34 - 36. (in Russian))

Fishman, Y.A. and E.G. Gaziev, 1974. In-situ and Model Studies of Rock Foundation Failure in Concrete Blocks Shear Tests. Proc. of the 3rd Congress of ISRM, Denver. p595 - 607.

Jaeger, J.C., N.G.W. Cook and R. Zimmerman, 2007. Fundamentals of Rock Mechanics. Fourth edition. Willey-Blakwell. p488.

Hardy, H.R., R.Y. Kim, P. Stefanko and Wang, 1969. Creep and Microseismic Activity in Geological Materials. Proceedings of 11th Symposium on Rock Mechanics, Berkly, Balkema, Rotterdam. p372 - 413.

Hoek, E. 1968. Brittle failure of rock. In: Stagg, K.S. and O.C. Zienkevich (Eds), Rock Mechanics in Engineering Practice. London: John Wiley & Sons. p99 - 124.

Kuster, G.T. and M.N. Toksöz, 1974. Velocity and attenuation of seismic waves in two-phase media. Part I.

Theoretical formulations. Geophysics, **39**(**5**): 587 - 606.

Luth, S., T. Bohlen, R. Giese, S. Heider, S. Hock, S. Jetchny, U. Polom, S. Wadas and A. Rechlin, 2014. Seismic tomography and monitoring in underground structures: developments in the Freiberg Reiche Zeche underground lab (Freiberg, Germany) and their application in underground construction (SOUND). In: Weber, M. and U. Munich (Eds.), Tomography of the Earth's Crust: From Geophysical Sounding to Real-Time Monitoring: GEOTECHNOLOGIEN Science Report No. 21. Springer International Publishing Switzerland. p115 - 134. doi:10.1007/978-3-319-04205-3_7.

Mastitsky, A.K. and S.B. Kereselidze, 1989. Viyavlennye otkloneniya ingenerno-geologicheskikh usloviy ot prognozirujemykh na uchastkah stroitelstva Ingury, Hudony I Zhinvali HES. Sbornik nauchnykh trudov Hydroprojecta, **136**: 49 - 55.

Maghsoudi, A. and B. Kalantari, 2014. Monitoring instrumentation in underground structures. Open Journal of Civil Engineering, **4**: 135 - 146. doi: 10.4236/ojce.2014.42012.

Muller, L., 1963. Der Felsbau, Salzburg Erster Band. Teoretischer Teel: Ferdinand Enke Verlag Stutgart.

O'Connel, R.J. and B. Budiansky, 1974. Seismic velocities in dry and saturated cracked solids. J. Geoph. Res., **79**: 5412 - 5426.

Pacher, F., 1970. Deformability of Rock Masses: Mechanism and Character of Deformations. Effect of Loading and Time. Proc. of the 2nd ISRM Congr, Beograd. **4**: 213 - 219.

Philips, J., K. Plenkers, G. Gartner and L. Teichmann, 2015. On the potential of in-situ Acoustic Emission (AE) technology for the monitoring of dynamic processes in Salt Mines. In: Roberts, L., K. Mellegard and F. Hansen (Eds.), The Mechanical Behavior of Salt VIII. Rapid City, South Dakota, U.S.A. May 26–28, 2015. CRC Press, London. p89 - 98.

Roberts, L., K. Mellegard and F. Hansen, (Eds.) 2015. The Mechanical Behavior of Salt VIII, Rapid City, South Dakota, U.S.A. May 26–28, 2015. CRC Press, London. p137 - 144. doi: 10.1201/b18393-18.

Rock Engineering Book, 1997. Available at https://vulcanhammernet.files.wordpress.com/2017/01/rock-engineering.pdf

Rudyak, M.S., 1996. Exploitation of the Methodology and Some Results of the Acoustic-emission Control for the Development of Rock Pressure on Lining of Hydrotechnical Tunnels. Ph.D. Thesis. Hydroproject Institute, Moscow. p132.

Salganik, R.L., 1979. Mechanics of bodies with many cracks. Mech. Solids, Engl. Transl., **8**: 135 - 143.

Savich, A.I., V.I. Koptev, B.N. Nikitin and Z.G. Yaschenko, 1969. Seismic-acoustic methods for study of the rock masses. Nedra Publishers, Moscow. p239. (In Russian)

Savich, A.I., M.M. Iliin, M.G. Ezersky and N.I. Kalinin, 1983. Long-term Geophysical Observations on the Inguri Dam Rock Foundation. Bull. of the EAEG No 26-27, Paris. p315 - 319.

Savich, A.I. and B.D. Kujundjich, (Eds). 1990. Complex Engineering-geophysical Explorations at the Hydrotechnical Construction. Moscow: Nedra. (in Russian)

Scholz, C.N., 1968. Microfracturing and the inelastic deformation of rock in compression. Journ. Geoph. Res., **73**(**4**): 1417 - 1432.

Spies, T., J. Hesser, J. Eisenblatter and G. Eilers, 2005. Measurement of acoustic emission during backfilling of large excavations. In: Potvin, Y. and M. Hudima (eds.), Proc. 6th Symp. Rocbursts and Seismicity in Mines (RaSiM 6). Australian Centre for Geomechanics, Australia. p379 - 383.

Stavrogin, A.N. and A.G. Protosenya, 1979. Plasticity of Rocks. Nedra Publishers, Moscow. p301. (in Russian).

Stavrogin, A.N. and A.G. Protosenya, 1983. Rock plasticity in conditions of variable deformation rates. Journal of Mining Science, **19**(**4**): 245 - 255.

Terzaghi, K. and F.E. Richart, 1952. Stresses in rock about cavities. Geotechnique, **3**: 57 - 90.

Terentiev, V.A., 1993. Compact Field Impulsive Ultrasonic Meter S-70. USSR Acad. Sci. Izv. Phys. Earth Ser. **11**: 54 - 57.

Vinogradov, S.D., K.M. Mirzoev and N.G. Salomov, 1975. Issledovanie Seysmicheskogo Rezhima Pri Razrushenii Obraztsov. Donish, Dushanbe. p117.

Yamamoto, Y. and M. Ito, 1993. New in situ Measurement Methods for Estimating Expansion of the Loosened Zone in Rock around a Large Cavern. Eurock'93, Lisboa, Portugal. Proc. ISRM Intern. Symp. June 21–24, 1993. Rotterdam, Balkema. p743 - 750.

Yu, X., C.D. da Gama, Y. Na, Q. Wang and Q. Xie, 2005. Deformation behaviour of rocks under compression and direct tension. The Journal of the South African Institute of Mining and Metallurgy, **105**: 55 - 62.

Zienkiewicz, O.C., 1968. Continuum mechanics as an approach to rock mass problems. In: Stagg, K.S. and O.C. Zienkewicz (Eds), Rock Mechanics in Engineering Practice. London: John Wiley & Sons. p237 - 273.

Zienkiewicz, O.C., R.L. Taylor and D. Fox. 2014. The Finite Element Method for Solid and Structural Mechanics. Seventh edition. Butterworth Heinemann, Oxford, USA, Elsevier.